

One-dimensional spin modulation in a charge ordered cuprate

N. B. Christensen,^{1,2} H. M. Rønnow,¹ J. Mesot,¹ R. A. Ewings,³ N. Momono,⁴ M. Oda,⁴ M. Ido,⁴ M. Enderle,⁵ D. F. McMorrow,^{6,7} and A. T. Boothroyd³

¹ *Laboratory for Neutron Scattering, ETH Zürich and PSI Villigen, CH-5232 Villigen PSI, Switzerland*

² *Materials Research Department, Risø National Laboratory, DK-4000 Roskilde, Denmark*

³ *Department of Physics, Oxford University, Oxford, OX1 3PU, United Kingdom*

⁴ *Department of Physics, Hokkaido University, Sapporo 060-0810, Japan*

⁵ *Institut Laue-Langevin, BP 156 - 38042 Grenoble Cedex 9 - France*

⁶ *London Centre for Nanotechnology and Department of Physics and Astronomy, University College London, UK*

⁷ *ISIS Facility, Rutherford Appleton Laboratory, Chilton, Didcot, UK*

(Dated: May 25, 2019)

Using polarized neutron scattering we establish beyond reasonable doubt that the magnetic order in $\text{La}_{1.48}\text{Nd}_{0.4}\text{Sr}_{0.12}\text{CuO}_4$ is one-dimensionally modulated and collinear. This observation is consistent with the stripe model and rules out a number of alternative models characterized by 2D electronic order or 1D helical spin order. The low energy spin excitations of the stripe ordered state are found to be primarily transversely polarized, consistent with conventional spin waves.

PACS numbers: 74.72.Dn, 75.30.Fv, 75.50.Ee, 75.70.Kw

One of the most striking and robust features in the phenomenology of the hole-doped copper oxide superconductors is the observation by neutron scattering of a fourfold pattern of incommensurate (IC) magnetic peaks centered on the antiferromagnetic (AFM) wavevector of the square CuO_2 lattice. This pattern is found in the magnetic excitation spectrum of $\text{YBa}_2\text{Cu}_3\text{O}_{6+y}$ and $\text{La}_{2-x}(\text{Sr},\text{Ba})_x\text{CuO}_4$ over a wide range of doping [1]. Furthermore, near $x = 1/8$ in certain materials the IC magnetic scattering develops an elastic component accompanied by second order harmonics around the structural Bragg peaks [2, 3]. One influential school of thought holds that these features are associated with one-dimensional (1D) charge modulations separating narrow AFM antiphase domains on the copper–oxygen layers [4]. In this ‘stripe’ model the fourfold pattern is interpreted as a superposition of two twofold patterns at right angles to one another, arising from spatially separated stripe domains, each with charge modulations aligned along one of the two Cu–O bond directions. Static stripes, posited to occur near $x = 1/8$, are believed to compete with superconductivity [5], but there are several theoretical scenarios in which dynamic stripes play a central role in the formation of the superconducting state [6].

Recently, however, the stripe picture has been called into question. Several new experimental findings point to the existence of 2D spin and/or charge density wave order in the ground state of hole-doped cuprates. These include scanning tunneling microscopy observations of checkerboard spatial modulations in the density of electronic states [7] and the appearance of resistivity anomalies in the normal state of $\text{La}_{2-x}\text{Sr}_x\text{CuO}_4$ at certain ‘magic’ doping fractions [8]. In addition, the dimensionality of the spin excitation spectrum is a subject of current debate [9]. Furthermore, an increasing number of phases exhibiting novel 2D electronic order have been explored

theoretically [10], including orbital current correlations [11], checkerboard-type orderings of Cooper pairs [12], and 2D diagonal stripes [13]. The possibility that features previously attributed to stripes might in fact be signatures of a more elaborate 2D ordering makes it vital to perform further investigations with experimental probes sensitive to the spatial arrangement of spin and charge.

In this Letter we report a study of the magnetic order and dynamics in spin and charge ordered tetragonal $\text{La}_{1.6-x}\text{Nd}_{0.4}\text{Sr}_x\text{CuO}_4$ (LNSCO; $x = 0.12$, $T_c = 6.8$ K)

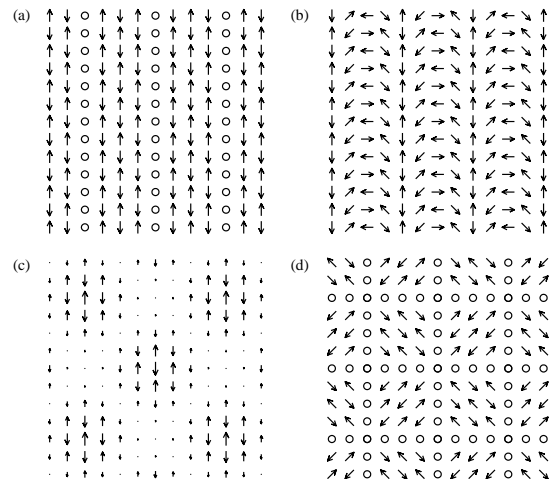


FIG. 1: Models for the magnetic order in the CuO_2 planes of superconducting La-based cuprates at $x = 1/8$ doping. (a) One- \mathbf{q} domain with charge stripes (lines of open circles) and collinear spin order [2]. (b) One- \mathbf{q} domain with helical spin order. (c) Collinear two- \mathbf{q} structure resulting from diagonal modulations of a commensurate antiferromagnet [13]. (d) Two- \mathbf{q} spin and charge ordering with non-collinear spin structure.

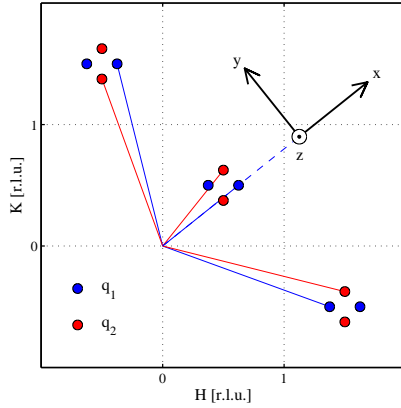


FIG. 2: Reciprocal space of the square CuO_2 lattice showing the three quartets of magnetic Bragg peaks investigated. The magnetic peaks are displaced from AFM wavevectors by $\pm \mathbf{q}_1$ and $\pm \mathbf{q}_2$ with $\mathbf{q}_1 = (\delta, 0)$ and $\mathbf{q}_2 = (0, \delta)$ ($\delta \simeq 0.12$). The magnetic cross-section can be resolved into contributions M_x and M_y from in-plane spin components along and perpendicular to the scattering vector \mathbf{Q} , respectively, and a contribution M_z from components perpendicular to the plane. For electronic spins, M_x is identically zero [16].

by polarised neutron scattering. This technique makes it possible to distinguish between alternative 1D and 2D models proposed to explain the fourfold pattern of IC magnetic peaks. We find that the results are most naturally understood in terms of a 1D modulation of the AFM order, consistent with the occurrence of stripes.

Figure 1 shows four models that yield magnetic diffraction patterns with principal Fourier components $\mathbf{Q} = (1/2, 1/2) \pm \mathbf{q}_1$ and $(1/2, 1/2) \pm \mathbf{q}_2$ and equivalent wavevectors (Fig. 2), as observed in a number of hole-doped compounds of La_2CuO_4 . Figure 1(a) is a schematic representation of the conventional view [2] that the quartet is produced by incoherent superposition of scattering from two domains, each with collinear one- \mathbf{q} , spin order. From the peak positions alone, this model is indistinguishable from a model involving two domains, each with helical one- \mathbf{q} order [14] as schematically shown in Fig. 1(b). These two models assume an equal population of domains with orthogonal propagation wavevectors. The correct four-fold diffraction pattern is also produced by the collinear two- \mathbf{q} “diagonal stripe” picture [13] in Fig. 1(c), and by the non-collinear, two- \mathbf{q} checkerboard structure shown in Fig. 1(d).

Our experiment was performed on the IN20 triple-axis spectrometer at the ILL operated in Heusler-Heusler configuration with a PG filter to suppress higher order contamination of the scattered beam. The crystal, which was grown by the floating-zone method, contained two grains separated by ~ 1 deg. The sample was mounted in a He cryostat with the [001] axis vertical. With a neutron energy of 34.8 meV, this configuration allowed access to IC quartets surrounding several equivalent AFM wavevec-

tors in the $(H, K, 0)$ reciprocal lattice plane, hereafter (H, K) for short. The polarisation vector \mathbf{P} of the neutron beam at the sample position could be oriented either in the horizontal scattering plane along or perpendicular to \mathbf{Q} (the neutron scattering vector), or out of the scattering plane (x , y and z -polarisation, respectively, Fig. 2). The scattered neutrons were recorded in spin-flip (SF) and non-spin-flip (NSF) channels, according to whether their spins had flipped or not on scattering.

The total cross-section for scattering of polarised neutrons consists of a purely nuclear term, a purely magnetic term and a nuclear-magnetic interference term [15]. We assume that the latter can be neglected at the IC wavevectors of interest, and that the nuclear spins are unpolarised. The magnetic contribution to the cross-section contains two features that make it possible to determine electronic spin directions. First, magnetic scattering originates only from electronic spin components \mathbf{S}_\perp perpendicular to \mathbf{Q} . Second, SF scattering is caused by spin correlations perpendicular to \mathbf{P} [15]. The cross-section is the sum of the normal, polarisation-independent term, proportional to $\mathbf{S}_\perp(\mathbf{Q}) \cdot \mathbf{S}_\perp(-\mathbf{Q})$ and a polarisation-dependent chiral term proportional to $\mathbf{P} \cdot (\mathbf{S}_\perp(\mathbf{Q}) \times \mathbf{S}_\perp(-\mathbf{Q}))$ [15]. A finite chiral term should reveal itself in the total, SF+NSF, scattering as an excess of intensity for x -polarisation relative to y and z -polarisation. At all IC wavevectors studied at 10 K the chiral contribution vanishes within the experimental error. To proceed, we denote coherent nuclear scattering by N and use the notation M_x , M_y and M_z for magnetic scattering from spin components in the scattering plane (M_x and M_y) and perpendicular to it (M_z), respectively, see Fig. 2. With background levels B_{SF} and B_{NSF} for the SF and NSF channels, the total cross-section for each of the six channels in the absence of chiral contributions can then be written as $I_{\text{SF}}^x = M_y + M_z + B_{\text{SF}}$, $I_{\text{SF}}^y = M_z + B_{\text{SF}}$, $I_{\text{SF}}^z = M_y + B_{\text{SF}}$, $I_{\text{NSF}}^x = N + B_{\text{NSF}}$, $I_{\text{NSF}}^y = N + M_y + B_{\text{NSF}}$ and $I_{\text{NSF}}^z = N + M_z + B_{\text{NSF}}$. These expressions apply both to elastic and inelastic scattering

We first consider elastic scattering, in which case M_y , M_z are proportional to the squares of the corresponding ordered moment components. At each of the three IC quartets indicated in Fig. 2, the neutron count rate was recorded in some or all six polarisation channels at each temperature. The advantage of probing several zones is that when the orientation of \mathbf{Q} is varied relative to the fixed direction of the ordered moments, the magnetic cross-sections M_y and M_z change. In LNSCO ($x = 0.12$), the Cu spins order below ~ 60 K. Coupling to the Cu spins causes the Nd spins to order below $T_{\text{Nd}} \simeq 3$ K. The Nd spin order is characterised by the same four wavevectors as the Cu spin order [17]. As we are primarily interested in the physics of the copper spins, the majority of our measurements were performed at 10 K $> 3 T_{\text{Nd}}$, but data were also taken at 1.7 K in order to determine the peak lineshapes, as described below.

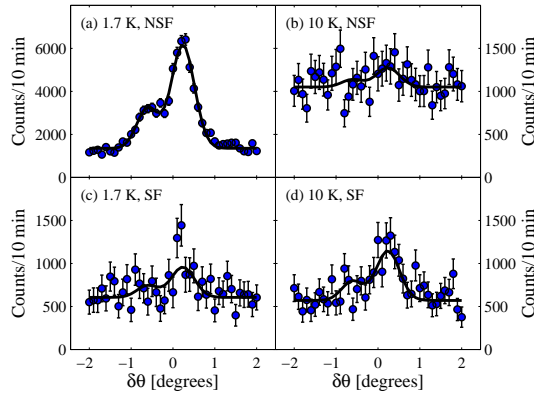


FIG. 3: Elastic magnetic scattering at $(1/2, 1/2) + \mathbf{q}_1$ with $\mathbf{P} \parallel z$ in the SF and NSF channels. The data have been corrected for imperfect beam polarisation, $P = 0.86$. Notice that the intensity scale in (a) differs from that of panels (b)–(d). The 2-peak line shape is due to the presence of two crystallites separated by ~ 1 deg. The solid line in (a) is a fit to a two-Gaussian lineshape. After fixing the positions, widths and relative amplitudes of the peaks, the lines in (b)–(d) were obtained by fitting only an overall intensity scale and a background.

Figure 3 shows data obtained by scanning the sample rotation angle θ through the $(1/2, 1/2) + \mathbf{q}_1$ satellite peak with z -polarisation. The SF and NSF channels are then sensitive to M_y and M_z respectively. The presence of a large peak in the NSF scattering shown in Fig. 3(a) implies that at 1.7 K, there is significant elastic scattering from magnetic moments oriented perpendicular to the CuO_2 planes. Heating to 10 K causes the peak in the NSF channel almost to vanish (Fig. 3(b)). A very weak peak is present in the SF channel at both 1.7 K and 10 K (Figs. 3(c) and (d)), centred on the position of maximum intensity in the 1.7 K NSF channel (Fig. 3(a)). These observations directly confirm the earlier deduction that the Nd moments order along \mathbf{c} [17]. Analysis of the data in Figs. 3(b) and (d) indicates that at 10 K, the direction of the moments giving rise to scattering is mainly confined to the CuO_2 planes. The data do not rule out a small ordered component along \mathbf{c} , but since the presence or absence of such a component does not alter our conclusions, we shall henceforth assume that at 10 K the Cu moments lie within the CuO_2 planes.

Next we turn to the spatial arrangement and in-plane orientation of the Cu moments at 10 K. Figure 4 shows M_y at three IC peaks of type \mathbf{q}_1 and at three peaks of type \mathbf{q}_2 . The \mathbf{q}_1 and \mathbf{q}_2 peaks close to $(1/2, 1/2)$ have roughly equal intensity (Figs. 4(a) and (b)). By contrast, there are significant intensity differences between the \mathbf{q}_1 and \mathbf{q}_2 peaks near both $(-1/2, 3/2)$ and $(3/2, -1/2)$ (Figs. 4(c)–(f)). Crucially, whereas near $(-1/2, 3/2)$ the \mathbf{q}_1 peak is clearly weaker than the \mathbf{q}_2 peak, the situation is reversed near $(3/2, -1/2)$.

The primary factors determining the relative intensi-

ties of IC peaks are the domain populations, and the orientations of the ordered spins $\langle \mathbf{S} \rangle_j$ of domain j relative to \mathbf{Q} . Since the angle between \mathbf{Q} and the unique spin direction of the single-domain, collinear two- \mathbf{q} model in Fig. 1(c) changes only slightly between the \mathbf{q}_1 and \mathbf{q}_2 peaks in any given zone, the large intensity differences observed near $(-1/2, 3/2)$ and $(3/2, -1/2)$ (Figs. 4(c)–(d) and (e)–(f)) cannot be reproduced by this model. For two such domains with orthogonal $\langle \mathbf{S} \rangle_j$ one expects equal intensities at all satellite peaks. The same is true for a two-domain, one- \mathbf{q} model based on in-plane helical (cycloidal) order (Fig. 2(b)), while any helix involving spin components perpendicular to the CuO_2 planes would give rise to a chiral term in the magnetic cross-section, in disagreement with our observations. Thus we can rule out both diagonal stripes and helical order.

By contrast, the data are qualitatively consistent with the existence of two one- \mathbf{q} domains, each with collinear spin order and with $\langle \mathbf{S} \rangle_j$ approximately perpendicular to \mathbf{q}_j as shown for one domain in Fig. 1(a). In this scenario, the \mathbf{q}_1 and \mathbf{q}_2 peaks near $(1/2, 1/2)$ have nearly identical intensities because the angle between \mathbf{Q} and $\langle \mathbf{S} \rangle_j$ is the same for both domains. On the other hand, near $(-1/2, 3/2)$, the \mathbf{q}_1 (\mathbf{q}_2) peak is relatively weak (strong)

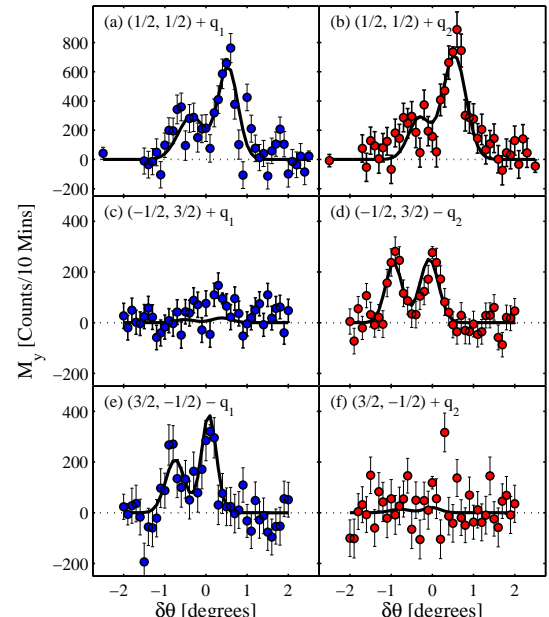


FIG. 4: Processed polarised-neutron data taken at $T = 10$ K, showing the in-plane component M_y of the magnetic cross-section at each of six IC peaks of type \mathbf{q}_1 and \mathbf{q}_2 (left and right columns, respectively). The data were obtained by first recording a rocking curve scan in each of the six polarisation channels for each \mathbf{Q} connected to $(0, 0)$ by solid lines in Fig. 2. M_y was then calculated both from the SF data ($M_y = I_{\text{SF}}^x - I_{\text{SF}}^y$) and from the NSF data ($M_y = I_{\text{NSF}}^y - I_{\text{NSF}}^x$). After checking for consistency, the M_y data thus obtained were combined. The solid lines represent the model calculation described in the text.

Wavevector \mathbf{Q}	Cross-section component	Intensity
$(-1/2, 3/2) + \mathbf{q}_1$	M_y	7.4 ± 1.3
$(-1/2, 3/2) + \mathbf{q}_1$	M_z	9.9 ± 1.4
$(3/2, -1/2) - \mathbf{q}_1$	M_y	2.4 ± 1.1
$(3/2, -1/2) - \mathbf{q}_1$	M_z	7.6 ± 1.1
Excitation components relative to [010]		
Transverse, out-of-plane		8.8 ± 0.9
Transverse, in-plane		7.8 ± 1.4
Longitudinal, in-plane		1.7 ± 1.3

TABLE I: Processed inelastic ($\hbar\omega = 5$ meV) count rates per 10 minutes at $T = 10$ K. M_y and M_z were obtained from $I_{\text{SF}}^x - I_{\text{SF}}^y$ and $I_{\text{SF}}^x - I_{\text{SF}}^z$, respectively. The total time invested to obtain these data was 18 hours at $(-1/2, 3/2) + \mathbf{q}_1$ and 26 hours at $(3/2, -1/2) - \mathbf{q}_1$.

since the corresponding spins are close to being parallel (perpendicular) to \mathbf{Q} . Around $(3/2, -1/2)$ these angular factors switch, and the \mathbf{q}_1 peak should be the most intense, as observed. The solid lines in Fig. 4 are quantitative calculations based on this model. As in Fig. 3, the lineshape at each \mathbf{Q} was fixed by fitting the large Nd signal in I_{NSF}^z at 1.7 K. The corresponding curves were then multiplied by the modulation expected for in-plane spins $\langle \mathbf{S} \rangle_j$ perpendicular to \mathbf{q}_j and corrected for the difference in form factor between the Nd-dominated 1.7 K signal and the 10 K copper signal. Although the calculations do not agree in every detail, they clearly reproduce the salient features of the data. More quantitatively, a least-squares fit of the model using all the data in Fig. 4 results in $\langle \mathbf{S} \rangle_1 \perp \mathbf{q}_1$ and $\langle \mathbf{S} \rangle_2 \perp \mathbf{q}_2$ with an accuracy of $\pm 3^\circ$. Our diffraction data are thus consistent with an *incoherent* superposition of orthogonal stripe domains.

Interestingly, our data are also consistent with the two- \mathbf{q} structure shown in Fig. 1(d). This model is based on a *coherent* superposition of two orthogonal stripe domains, and produces the correct (i.e. observed) positions for both the charge and magnetic peaks. This has two implications. First, one cannot infer the existence of 1D stripes from existing measurements of charge and magnetic peak positions [2, 4], and second, although our results also do not rigorously rule out a checkerboard configuration, they do impose the spin arrangement shown in Fig. 1(d) on any such model. This arrangement seems physically unlikely since it is difficult (perhaps impossible) to construct an exchange Hamiltonian which would favor alternating clockwise and anticlockwise rotations of spin directions across charge lines.

In the case of inelastic scattering, M_z is sensitive to magnetic fluctuations out of the scattering plane and M_y to in-plane fluctuations perpendicular to \mathbf{Q} . Table I shows the M_y and M_z count rates at $(-1/2, 3/2) + \mathbf{q}_1$ and $(3/2, -1/2) - \mathbf{q}_1$ at $\hbar\omega = 5$ meV (The counting times were too long to perform full \mathbf{Q} -scans through the magnetic peaks). Within the errors, M_z is the same for the \mathbf{q}_1 peaks in both zones, as expected for ordered

moments confined to the scattering plane. By contrast, there is a statistically significant difference between the values of M_y at the two wavevectors. This shows that the spin fluctuations in LNSCO have a preferred direction, and implies that they are not of the singlet-triplet type for which we would expect $M_y = M_z$ at each \mathbf{Q} . Instead, the simultaneous observations (compare Table I and Fig. 4(c) and (e)) of a relatively small (large) elastic M_y and a relatively large (small) inelastic M_y at $(-1/2, 3/2) + \mathbf{q}_1$ ($(3/2, -1/2) - \mathbf{q}_1$), find a natural explanation when referred to the \mathbf{q}_1 stripe domain shown in Fig. 1(a) for which the inelastic M_y at $(-1/2, 3/2) + \mathbf{q}_1$ and $(3/2, -1/2) - \mathbf{q}_1$ are dominated by fluctuations transverse to and along $\langle \mathbf{S} \rangle_1$, respectively. Converting from M_y to components transverse to and along $\langle \mathbf{S} \rangle_1$ shows (Table I) that the fluctuations are predominantly transverse, consistent with spin wave modes. This finding supports theories of the cuprate excitation spectrum which start from coupled ladders [18] and converge on the view that the excitations below the (commensurate) resonance energy are Goldstone modes of the particular microscopic order envisaged.

In summary, by combining the direct sensitivity of neutrons to the directions of ordered moments and fluctuations with the clean, background-free signal obtained with polarisation analysis, we conclude that in the known spin- and charge ordered compound $\text{La}_{1.48}\text{Nd}_{0.4}\text{Sr}_{0.12}\text{CuO}_4$ [2], the magnetic order is modulated in 1D only (with spins perpendicular to the modulation vector). It is then reasonable to conclude that the charge order must also be one-dimensional, consistent with a stripe interpretation.

NBC was supported by the Danish Natural Science Council via DanScatt and the Danish Technical Research Council under the Framework Program on Superconductivity. DFM was supported by a Wolfson Royal Society Research Merit Award. RAE was supported by a studentship from the Engineering & Physical Sciences Research Council of Great Britain. We thank J.P. Hill, J.M. Tranquada and S.A. Kivelson for stimulating discussions.

- [1] S-W. Cheong *et al.*, Phys. Rev. Lett. **67**, 1791 (1991); K. Yamada *et al.*, Phys. Rev. B **57**, 6165 (1998); H. A. Mook *et al.*, Nature (London) **395**, 580 (1998); P. Dai *et al.*, Phys. Rev. B **63**, 054525 (2001).
- [2] J. M. Tranquada *et al.*, Nature (London) **375**, 561 (1995).
- [3] M. Fujita *et al.*, Phys. Rev. B **66**, 184503 (2002); M. Fujita *et al.*, Phys. Rev. B **70**, 104517 (2004);
- [4] S. A. Kivelson *et al.*, Rev. Mod. Phys. **75**, 1201 (2003).
- [5] A. R. Moodenbaugh *et al.*, Phys. Rev. B **38**, 4596 (1988); K. Kumagai *et al.*, J. Magn. Magn. Mater. **76–77**, 601 (1988); J. M. Tranquada *et al.*, Phys. Rev. Lett. **78**, 338 (1997).
- [6] V. J. Emery, S. A. Kivelson, and O. Zachar, Phys. Rev. B **56**, 6120 (1997); Yu. A. Krotov, D. -H. Lee, and A. V.

Balatsky, Phys. Rev. B **56**, 8367 (1997); H. Johannesson and G. I. Japaridze, Phys. Rev. B **68**, 214507 (2003).

[7] J. E. Hoffman *et al.*, Science **295**, 466 (2002); T. Hanaguri *et al.*, Nature (London) **430**, 1001 (2004).

[8] A. Komiya *et al.*, Phys. Rev. Lett. **94**, 207004 (2005).

[9] S. M. Hayden *et al.*, Nature (London) **429**, 531 (2004); J. M. Tranquada *et al.*, Nature (London) **429**, 534 (2004); N. B. Christensen *et al.*, Phys. Rev. Lett. **93**, 147002 (2004); V. Hinkov *et al.*, Nature (London) **430**, 650 (2004); P. Bourges *et al.*, Science **288**, 1234 (2000); C. Stock *et al.*, Phys. Rev. B **71**, 024522 (2005).

[10] S. Sachdev, Science **288**, 475 (2000).

[11] X. G. Wen and P. A. Lee, Phys. Rev. Lett. **76**, 503 (1996); C. M. Varma, Phys. Rev. B **55**, 14554 (1997); S. Chakravarty *et al.*, Phys. Rev. B **63**, 094503 (2001).

[12] M. Vojta, Phys. Rev. B **66**, 104505 (2002); H. D. Chen *et al.*, Phys. Rev. Lett. **93**, 187002 (2004); Z. Tesanovic, Phys. Rev. Lett. **93**, 217004 (2004); H.-X. Huang, F.-Q. Li and F.-C. Zhang, Phys. Rev. B **71**, 184514 (2005); P. W. Anderson cond-mat/0406038 (unpublished).

[13] B. V. Fine, Phys. Rev. B **70**, 224508 (2004).

[14] O. P. Sushkov and V. N. Kotov, Phys. Rev. B **70**, 024503 (2004); P.-A. Lindgård, Phys. Rev. Lett. **95**, 217001 (2005).

[15] R. M. Moon and T. Riste and W. C. Koehler, Phys. Rev. **181**, 920 (1969).

[16] G. L. Squires, *Introduction to the Theory of Thermal Neutron Scattering*, Dover Publications, Inc., 1996.

[17] J. M. Tranquada *et al.*, Phys. Rev. B **54**, 7489 (1996).

[18] M. Vojta and T. Ulbricht, Phys. Rev. Lett. **93**, 127002 (2004); G. S. Uhrig, K. P. Schmidt, and M. Grüninger, Phys. Rev. Lett. **93**, 267003 (2004); M. Vojta and S. Sachdev, J. Phys. Chem. Solids **67**, 11 (2006); G. Seibold and J. Lorenzana, Phys. Rev. Lett. **94**, 107006 (2005); B. M. Andersen and P. Hedegård, Phys. Rev. Lett. **95**, 037002 (2005); D. X. Yao, E. W. Carlson and D. K. Campbell, Phys. Rev. Lett. **97**, 017003 (2006); M. Vojta, T. Vojta and R. K. Kaul, cond-mat/0510448